

## Strong field transient manipulation of electronic states and bands

I. Crassee, L. Gallmann, G. Gäumann, M. Matthews, H. Yanagisawa, T. Feurer, M. Hengsberger, U. Keller, J. Osterwalder, H. J. Wörner, and J. P. Wolf

Citation: [Structural Dynamics](#) **4**, 061505 (2017); doi: 10.1063/1.4996424

View online: <https://doi.org/10.1063/1.4996424>

View Table of Contents: <http://aca.scitation.org/toc/sdy/4/6>

Published by the [American Institute of Physics](#)

---

### Articles you may be interested in

[Photoemission and photoionization time delays and rates](#)

[Structural Dynamics](#) **4**, 061502 (2017); 10.1063/1.4997175

[Nonadiabatic effects in electronic and nuclear dynamics](#)

[Structural Dynamics](#) **4**, 061510 (2017); 10.1063/1.4996816

[Charge migration and charge transfer in molecular systems](#)

[Structural Dynamics](#) **4**, 061508 (2017); 10.1063/1.4996505

[Watching ultrafast responses of structure and magnetism in condensed matter with momentum-resolved probes](#)

[Structural Dynamics](#) **4**, 061506 (2017); 10.1063/1.4996176

[Perspective: THz-driven nuclear dynamics from solids to molecules](#)

[Structural Dynamics](#) **4**, 061601 (2017); 10.1063/1.4992050

[Femtosecond manipulation of spins, charges, and ions in nanostructures, thin films, and surfaces](#)

[Structural Dynamics](#) **4**, 061504 (2017); 10.1063/1.4995541

---

## Strong field transient manipulation of electronic states and bands

I. Crassee,<sup>1</sup> L. Gallmann,<sup>2,3</sup> G. Gäumann,<sup>2</sup> M. Matthews,<sup>1</sup> H. Yanagisawa,<sup>4</sup>  
 T. Feurer,<sup>2</sup> M. Hengsberger,<sup>4</sup> U. Keller,<sup>3</sup> J. Osterwalder,<sup>4</sup> H. J. Wörner,<sup>5</sup> and  
 J. P. Wolf<sup>1,a)</sup>

<sup>1</sup>Applied Physics, GAP, University of Geneva, 22 Ch. de Pinchat, 1211 Geneva 4, Switzerland

<sup>2</sup>Institute of Applied Physics, University of Bern, Sidlerstr 5, 3012 Bern, Switzerland

<sup>3</sup>Department of Physics, Institute for Quantum Electronics, ETH-Zurich, 8093 Zurich, Switzerland

<sup>4</sup>Department of Physics, University of Zurich, Winterthurerstr 190, 8057 Zurich, Switzerland

<sup>5</sup>Physical Chemistry Laboratory, ETHZ, Vladimir-Prelog-Weg 2, 8093 Zurich, Switzerland

(Received 17 July 2017; accepted 18 September 2017; published online 21 December 2017)

In the present review, laser fields are so strong that they become part of the electronic potential, and sometimes even dominate the Coulomb contribution. This manipulation of atomic potentials and of the associated states and bands finds fascinating applications in gases and solids, both in the bulk and at the surface. We present some recent spectacular examples obtained within the NCCR MUST in Switzerland. © 2017 Author(s). All article content, except where otherwise noted, is licensed under a Creative Commons Attribution (CC BY) license (<http://creativecommons.org/licenses/by/4.0/>). <https://doi.org/10.1063/1.4996424>

### I. INTRODUCTION

At intensities exceeding 10–100 TW/cm<sup>2</sup>, laser fields strongly compete with Coulomb binding potentials for driving electron and nuclear dynamics. The related Hamiltonian of the system then becomes time dependent, with a periodicity following the laser driving frequency  $\omega_0$ . In the Floquet analysis<sup>1</sup> framework, the solutions of the time dependent Schrödinger equation (TDSE) consist of linear combinations of stationary states with energies of the bare atom, “dressed” by the energies of the field photons. The Floquet approach is reminiscent, in the time domain, of the appearance of Bloch states and associated bands of electrons in a spatially periodic lattice potential.

In the simplest case, where  $\omega_0$  couples quasi-resonantly two levels of the bare atom (small detuning  $\Delta \ll \omega_0$ ), the dressed states form a doublet. The induced splitting  $\hbar(\Omega^2 + \Delta^2)^{1/2}$  is related to the well-known Rabi frequency  $\Omega = \mathbf{p} \cdot \mathbf{E}_0 / \hbar$ , where  $\mathbf{p}$  is the atomic dipole and  $\mathbf{E}_0$  is the laser field. The AC-Stark effect, at the origin of this splitting, was discovered in 1955 by Autler and Townes, in the microwave domain,<sup>2</sup> so that this splitting is named after the two famous scientists. For ultrashort pulses, the AC-Stark effect also induces a broadening of the lines, because of its time varying field envelope. In the general case, for strong fields, several states of the bare atom are mixed together by the optical field and can be detuned by as much as several times the driving frequency.<sup>3</sup> Recently, the Stark field induced manipulation of a molecular orbital shape could be directly mapped by monitoring the high harmonic generation (HHG) from pre-aligned and pre-oriented molecules, as a function of the laser field strength.<sup>4</sup> This experiment, performed by Wörner, constitutes one of the examples presented in this focus review (Sec. II).

The manipulation of atomic/molecular potentials and solid state bands by a strong external field can also be used for controlling electron dynamics. The most striking example relates to

<sup>a)</sup>jean-pierre.wolf@unige.ch

tunnel ionization and high harmonic generation, as reviewed in Keller *et al.*<sup>5</sup> For instance, in the celebrated 3-step model elaborated by Corkum,<sup>6</sup> the electron evolves in a time dependent potential that mixes the Coulomb atomic field with the field of the light wave. Beyond the semi-classical picture of an ionized electron re-colliding with its parent ion after having acquired ponderomotive energy, atomic states can become more stable when the strength of the laser field exceeds the Coulomb attraction to the ionic core. Initially proposed by theorists since the 1980s,<sup>7–11</sup> such stabilized states were indirectly inferred in experiments only 3 decades later,<sup>12,13</sup> showing the ability of isolated neutral atoms to survive laser intensities as high as  $I \sim 10^{15}–10^{16} \text{ W/cm}^2$ . Very recently, these “bound states of free electrons,” also known as “Kramers-Henneberger (KH) states” have been observed in laser filaments<sup>14</sup> at significantly lower intensities. In this particular geometry, KH states even contributed to the stabilization of the filamentation process, as presented in Sec. III of this review.

On the other hand, the free electrons emitted after re-scattering of the ions also carry fascinating features. Here, we will focus (Sec. IV) on the example of ultrafast optical field emission from a DC-biased metal tip, where a strong laser field bends the surface barrier and drives the electrons through it, producing attosecond coherent electron waves.<sup>15–18</sup> In particular, the group of Osterwalder showed that the energy loss and the phase delay acquired by the electrons during the re-scattering process reveal information on multi-electron interactions and on the structure of the metal at and below the surface.<sup>18</sup>

Strong field manipulation of potential energy surfaces also provides control over processes other than ionization, namely, selective bond breaking, charge transfer, and conformational change. The concept of light-induced potentials (LIP)<sup>19–24</sup> was introduced in the 1990s for explaining processes like bond softening (of the ground state) or hardening (of a dissociative state), and selective vibronic population transfer by adiabatic passage (APLIP). More recently, dynamic Stark effects were used to generate light-induced avoided crossings (LIAC) between potential energy surfaces or light-induced conical intersections (LICI).<sup>25–31</sup> For example, LICI proved efficient in controlling the yield of photoisomerization in hydrocarbons,<sup>31</sup> as well as the branching ratio of a reaction in a polyatomic molecule<sup>27,28</sup> including efficient bond breaking in the ground state.

In solids, similar effects like Rabi oscillations in atoms arise from the periodicity of the potential under strong field coupling, namely, Bloch oscillations (see, e.g., Refs. 75,116,117). The manipulation of the band structure by strong fields similarly leads to dynamic Stark shifting and bandgap modulation. Dressed bands can be constructed by the same Floquet approach as for atoms and molecules.<sup>32,33</sup> However, consequences may be different in solids than in molecules: for instance, the laser field can transiently mix valence and conduction bands, turning an insulator into a conductor with femtosecond switching speeds.<sup>34</sup> An additional fascinating effect is the acceleration of electron-hole pair intraband, the dynamic Franz-Keldysh effect, which results in induced transparency and side bands in the optical spectra. Keller’s group recently observed the Franz-Keldysh dynamics in diamond samples at attosecond time scales,<sup>35</sup> as described in Sec. V.

A particularly interesting case of band structures is obviously the Dirac cones in graphene and its analogs. In neutrally doped graphene, interband transitions can occur at any frequencies, leading to constant optical conductivity. By doping graphene, both intra-band and interband transitions become possible. The modulation of these properties by irradiating graphene with a strong electric field is therefore particularly attractive, especially close to the Dirac point. This investigation, consisting of strong THz field induced non-linearity in doped graphene constitutes the last example of this focus review.

## II. STARK-EFFECT INDUCED MANIPULATION OF MOLECULAR ORBITALS

The non-linearity of laser-matter interaction in the  $10–100 \text{ TW/cm}^2$  regime leads to the achievement of temporal resolution well below the duration of an optical cycle. This property has been exploited to resolve nuclear dynamics in laser-induced recollision,<sup>36,37</sup> high-harmonic spectroscopy<sup>38–40</sup> and laser-induced electron diffraction,<sup>41</sup> and to resolve electronic dynamics<sup>42,43</sup>

and charge migration<sup>44</sup> in high-harmonic spectroscopy. In most of these and related studies, the effects of the strong laser field on the electronic structure of the investigated molecule have been neglected.

In a recent study by the group of Wörner, first experimental evidence for laser-induced modifications of the electronic structure has been obtained.<sup>4</sup> In the experimental part of this work, high-harmonic emission from spatially aligned and oriented methyl halide molecules has been measured. In the theoretical part, the laser-induced modifications of the electronic structure have been included in all three steps of high-harmonic generation, i.e., ionization, electron propagation and recombination. The comparison of the experimental data with the complete theory on one hand and field-free theory on the other revealed the very pronounced effect of the laser electric field on the observables of high-harmonic spectroscopy.

Methyl fluoride ( $\text{CH}_3\text{F}$ ) and methyl bromide ( $\text{CH}_3\text{Br}$ ) have been impulsively aligned and oriented using ultrashort laser pulses. Alignment was achieved using temporally stretched non-resonant laser pulses centered at 800 nm. Orientation was realized by using a phase-controlled superposition of 800-nm and 400-nm laser pulses.<sup>45–47</sup> In all cases, high-harmonic emission was recorded as a function of the pump (alignment)–probe (HHG) delay around the full rotational revival of the molecules, and therefore well outside the temporal overlap region of the pump and probe pulses. Two experimental observables were extracted from these experimental data, i.e., the ratio of high-harmonic intensities for molecules aligned parallel or perpendicular to the polarization of the laser field driving HHG (aligned-to-anti-aligned ratio) and the intensity ratio of even harmonics (of order  $2q$ ) to their neighboring odd harmonics (of the order of  $2q \pm 1$ ).

Strong electric fields significantly modify the electronic structure of molecules. The electronic states of the molecule in the presence of an external electric field are shifted in energy by the Stark shift with respect to the field-free states. The new eigenstates are moreover expressed by linear combinations of the field-free states. Experimental evidence for these two effects has been obtained from high-harmonic spectra. The relevant orbitals in this study are the highest-occupied molecular orbitals (HOMO) of  $\text{CH}_3\text{F}$  [Fig. 1(a)] and  $\text{CH}_3\text{Br}$ , which are qualitatively very similar. The HOMOs have E symmetry in the  $\text{C}_{3v}$  point group and are degenerate in the absence of an external field. The application of a static electric field of 0.05 atomic units (corresponding to a laser peak intensity of  $8.8 \times 10^{13} \text{ W/cm}^2$ ) leads to a mixing of these two orbitals and a splitting of their binding energies [Fig. 1(b)]. This field-induced mixing of these orbitals and the associated energy shifts have been incorporated into the calculation of all three steps of high-harmonic emission for the first time. Briefly, the weak-field asymptotic theory (WFAT) has been extended to incorporate the Stark effect and has been used to calculate the strong-field ionization rates in the molecular frame. The Stark-effect coefficients have been obtained from all-electron *ab-initio* quantum chemical calculations with applied external fields. The Stark effect has also been taken into account in calculating the accumulated phase during the excursion of the electron in the continuum. The photorecombination matrix elements have been determined from state-of-the-art electron-molecule-scattering calculations. Finally, the high-harmonic emission calculated in the molecular frame has been averaged over the alignment distributions to obtain the predicted high-harmonic signal in the laboratory frame.

The results of the full theory including the laser-induced modification of the molecular orbitals are found to be in quantitative agreement with all experimental data. The case of aligned  $\text{CH}_3\text{Br}$  molecules [Fig. 1(c)] and oriented  $\text{CH}_3\text{F}$  molecules [Fig. 1(d)] are shown as illustrations. The prediction of the full theory lies outside the error bars of the two lowest data points. This is not surprising because these photon energies lie close to the respective ionization energies, where recollision-based theories are expected to fail.

Overall, this study demonstrates large and measurable effects arising from laser-induced modifications of molecular orbitals. It shows that the laser field driving HHG can significantly modify the electronic structure of molecules. These results suggest that intense laser fields could be used to control the electronic structure of molecules and thereby influence their properties at the time scales of laser-field oscillations.

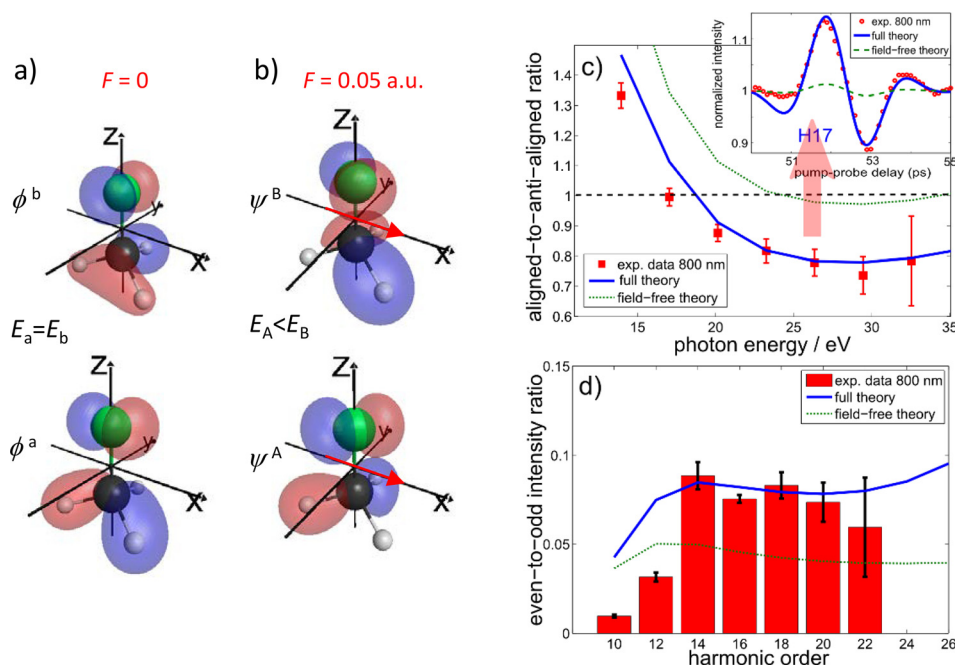


FIG. 1. Manifestation of the Stark-effect induced modification of molecular orbitals in high-harmonic spectroscopy. (a) Field-free highest-occupied molecular orbitals of CH<sub>3</sub>F belonging to the irreducible representation E of the C<sub>3v</sub> point group. (b) The two highest-occupied molecular orbitals of CH<sub>3</sub>F in the presence of a static electric field as obtained from an *ab-initio* quantum chemical calculation. (c) Intensity ratio of high harmonics emitted from aligned and anti-aligned CH<sub>3</sub>Br molecules compared to the full theory including the laser-induced effects and the field-free theory. (d) Intensity ratio of even and odd high harmonics emitted from oriented CH<sub>3</sub>F molecules compared to both theories. Reproduced with permission from Kraus *et al.*, Nat. Commun. 6, 7039 (2015). Copyright 2015 Springer Nature Publishing.

### III. BOUND STATES OF FREE ELECTRONS AND NON-LINEAR PROPAGATION

The deformation of atomic and molecular orbitals by strong fields also influences the propagation of high intensity lasers in transparent media. For instance, in air, when the peak power of a laser exceeds some GW, called “critical power”<sup>48</sup> the beam propagation becomes non-linear, and self-focusing occurs due to the optical Kerr effect. The polarization of the medium is then modified by a first order non-linear correction  $\chi^{(3)}I$  in the susceptibility tensor. However, when the intensity  $I$  reaches  $10^{13}$ – $10^{15}$  W/cm<sup>2</sup> (at 800 nm) the non-linear polarization  $P_{NL}(I)$  is not correctly approximated by a perturbative expansion anymore. This was recently illustrated by calculating the exact  $P_{NL}(I)$  function using *ab-initio* methods solving the time-dependent Schrödinger equation for hydrogen (Fig. 2), and fitting the result with a power series.<sup>49</sup> The best fit then clearly showed no convergence with increasing order, demonstrating the contradiction with a perturbative Taylor series expansion.

The coefficients of the best fit of the actual non-linear polarization on the intensity range of interest were first introduced as “higher order Kerr” (HOKE) terms.<sup>50</sup> This denomination turned out to be misleading in the community, because these coefficients were directly compared to the coefficients of a converging Taylor expansion (and thus a perturbative treatment) instead of a local polynomial fit. This misunderstanding led to a controversy in the laser filamentation community some years ago. In filamentation, the negative and positive non-linear contributions to the polarization indeed compensates, leading to self-stabilization in the propagation regime and to narrow “strings” of light which can propagate over hundreds of meters.<sup>48</sup> Notice that the non-linear polarization affecting propagation is also the source term of the high harmonic generation process, which creates a bridge between both communities (filamentation and HHG).<sup>51</sup>

An interesting interpretation of the  $P_{NL}(I)$  saturation was recently proposed by the groups of Ivanov and Smirnova in terms of atomic stabilization and Kramers-Henneberger states.<sup>52,53</sup>

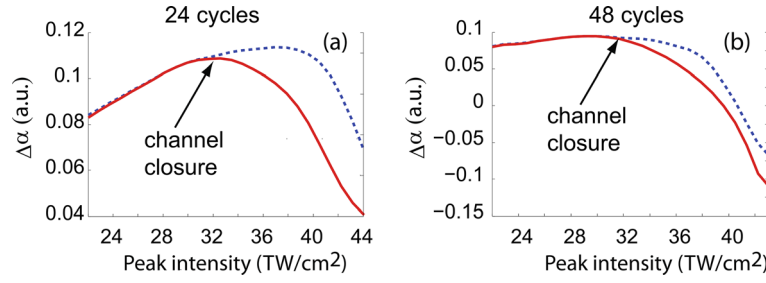


FIG. 2. Atomic non-linear polarizability in high fields for shorter (a) and longer (b) optical waveforms. For intensities of up to  $30 \text{ TW/cm}^2$ , the linear response with intensity, expressing the usual  $\chi^{(3)}$  induced Kerr focusing is observed. Above, the polarization saturates and even reverses sign, revealing the departure from the perturbative Taylor expansion regime. The blue dashed lines represent a model including the  $\chi^{(3)}$  induced Kerr focusing only, but with an *ad-hoc* addition of a negative contribution from free electrons. Reproduced with permission from B  jot *et al.*, Phys. Rev. Lett. **110**, 043902 (2013). Copyright 2013 American Physical Society.

More precisely, at high frequencies and strong fields, Floquet theory successfully describes the ladder of dressed or quasi energy states, which can form above the ionisation potential,<sup>54,55</sup> and which possess both bound and free electron characteristics. It is thus appealing to apply a variable transformation into the oscillating reference frame of the electron in the strong driving field, leading to Kramers-Henneberger (KH) potential.<sup>8,56,57</sup> For a hydrogenic system, solving the resulting TDSE in this reference frame produces a series of strongly modified—stable—states.<sup>7,8,52,53</sup> Conceptually, the electron can be considered to feel a cycle-averaged dressed, oscillating ionic potential. The new “KH” states are significantly different from the field free atomic set and endure for the duration of the driving laser pulse, as shown, for example, in Fig. 3. Notice that atomic stabilization (i.e., ionization frustration) has recently been observed experimentally in Rydberg states from He atoms, which survived ionization from optical fields of 6 orders of magnitude larger than the binding energy.<sup>13,58</sup>

Recent studies, using both *ab initio* calculations<sup>59,60</sup> and Floquet analysis,<sup>54,55</sup> confirm that at intensities in the region of  $10^{14} \text{ W/cm}^2$  and near infrared (NIR), these stable dressed states arise. Populating these states requires a pulse with a sharp rise time because a gradual risetime, e.g., a Gaussian shape, leads to exceptionally short lifetimes of the dressed states, due to the transition from a perturbative to a strong field regime.<sup>52,53</sup> A shaped NIR pulse with a sharp ( $\sim$ single cycle) edge enables the rapid transfer of population, and a flat top means the laser-dressed states are preserved, with a well-defined Stark shift. These Stark-shifted Rydberg states are stable against ionisation. The resonances on KH states thus lead to not only absorption, but also to a change in the real part of the susceptibility tensor, and thus saturation of the non-linear

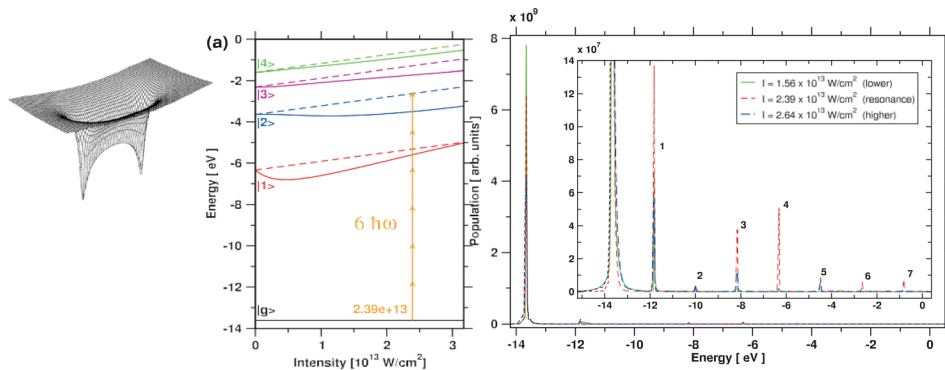


FIG. 3. (a) Kramers-Henneberger potential felt by an electron in its own reference frame. Reproduced with permission from Eberly and Kulander, Science, **262**(5137), 1229–1233 (1993). Copyright 1993 AAAS. (b) *Ab-initio* calculations of KH state energies in the case of hydrogen and quasi energy spectra (c) expected from the ground state. Reproduced with permission from Richter *et al.*, New J. Phys. **15**(8), 083012 (2013). Copyright 2013 IOP under Creative Commons.



refractive index.<sup>61</sup> By performing the associated calculation, Ivanov *et al.*<sup>52</sup> could retrieve almost exactly the saturation behavior of Fig. 2, shedding new light on the origin of the HOKE effects.

The distinct spectral signatures of KH states could be recently observed by shaping laser filaments in noble gases, (3–9 bar),<sup>14</sup> at guiding intensities of  $\sim 10^{14}$  W/cm<sup>2</sup>. These spectral signatures, which distinctly depend on the pulse rise time, duration and intensity demonstrate that dressed, “KH” states can be efficiently populated. Electrons trapped in these states respond almost as free, yet they remain bound and contribute to the intensity dependence of the non-linear refractive index of the medium, in which the laser propagates.<sup>62</sup>

#### IV. STRONG OPTICAL FIELD EMISSION FROM SURFACES

Ultrafast nano-electronic devices operating on femto- to atto-second timescales have received considerable attention as candidates for devices with an unprecedented operating speed.<sup>15,34</sup> These devices rely on ultrafast electron dynamics in nano-objects driven by ultrashort laser pulses. In particular, illuminating a nanostructure with a strong-field laser drives attosecond processes such as rescattering emission,<sup>16</sup> quivering motion,<sup>17</sup> or subcycle emission,<sup>17</sup> which would play a central role in attosecond electronic devices. On the downside, strong-field laser pulses induce multiple-electron emission from metallic condensed matter, which blurs important physics due to mutual Coulomb repulsion. Analyzing the kinetic energy spectra of emitted electron currents, the opening of a new emission channel associated with strong-field effects could recently be observed.<sup>18</sup> In this section, we shall review the complicated ultrafast electron dynamics that are peculiar to metallic nanostructures.

Applying strong DC electric fields to a metallic tip leads to field emission due to electrons from near the Fermi energy tunneling into a vacuum.<sup>63</sup> Field emission is widely used for producing highly coherent electron beams because of their inherently small, nanoscale source size.<sup>64,65</sup> Illuminating such a nano-tip with femtosecond laser pulses induces laser-assisted pulsed field emissions as schematically illustrated in Fig. 4(a), which generates coherent electron pulses from nanoscale areas.<sup>65–67</sup> Optical electric fields are enhanced at the tip apex due to the excitation of surface electromagnetic waves such as, e.g., surface plasmon polaritons.<sup>68</sup> Depending on the strength of the enhanced field, different emission processes become dominant. For relatively weak fields, single-electron excitations by single- or

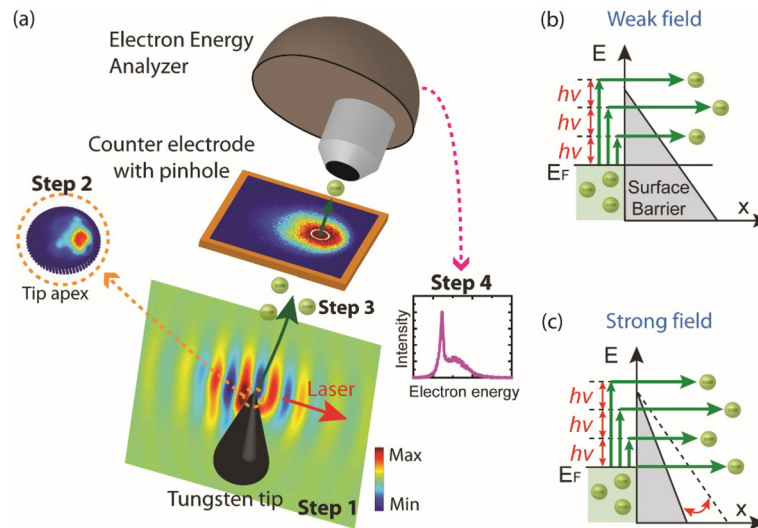


FIG. 4. (a) Simulation steps for electron emission from a tungsten tip illuminated by a focused laser beam. The longitudinal cross-section gives the field of the laser pulse when its maximum hits the tip apex (Step 1). Plasmonic effects lead to a local field enhancement on the shadow side of the tip (Step 2) which leads to laser-assisted field emission (Step 3), imaged at the counter electrode. A pinhole admits electrons into a hemispherical energy analyzer for recording the kinetic energy spectrum (Step 4). Illustration of different emission mechanisms in the weak (b) and strong (c) field regimes. Adapted with permission from Yanagisawa *et al.*, Sci. Rep. 6, 35877 (2016). Copyright 2016 Springer Nature Publishing.

multi-photon absorption are prevalent. Emission follows as photoexcited electrons tunnel through the surface potential barrier or are emitted over the barrier, as shown in Fig. 4(b).<sup>69,70</sup> In contrast, strong optical fields modify the surface barrier and induce field emission even from the Fermi level, as seen in Fig. 4(c).<sup>16–18</sup> This emission process, called *optical field emission*, has gained wide attention because it produces coherent attosecond electron waves due to its sensitivity to the phase of the laser pulse.

The transition from the weak to the strong field regime was studied recently by Yanagisawa *et al.* by using 7 fs laser pulses of increasing peak intensity and by analyzing the evolution of the kinetic energy spectrum of the emitted electrons by means of an electron spectrometer as shown in Fig. 4(a). The resulting spectra in Fig. 4(a) show a smooth crossover from one regime to the other. A small peak associated with two-photon photoemission (2PPE) dominates the spectrum at the lowest laser power. With increasing laser intensity, the peak grows in intensity and its maximum gradually moves towards slightly lower energies. Concurrently, a plateau feature with nearly constant intensity grows sideways towards higher energies. Gray arrows indicate these two general trends. This behaviour is entirely different from that in the weak-field regime. Further analysis indicates that the behavior of the peak deviates from that of the 2PPE excitations. Figure 4(c) shows the peak intensities as a function of laser peak intensity in a log-log plot (open circles). 2PPE processes follow a straight line with a slope of two (dashed line), as observed in a similar dataset measured with 70 fs laser pulses (filled triangles) of up to about  $2 \times 10^{12} \text{ W/cm}^2$ . Beyond this laser intensity, the resulting peak evolution shows two kinks (green and red arrows). These kinks are strong indicators of changes in the emission process.

A direct interpretation of the observed spectroscopic signatures is complicated by strong multi-electron effects: several hundred electrons per pulse were emitted from the tip apex at higher laser intensities. To understand the physics behind the observed kinks, the emission processes described above were simulated. Within a laser pulse duration, multiple electron trajectories in a vacuum were calculated by mutual Coulomb repulsion taken into account. As schematically depicted in Fig. 4(a), the simulations consisted of four steps. In the first step, temporal and spatial evolution of the optical fields near the tip were computed with including plasmonic effects by solving Maxwell's equations based on the Multiple Multipole Program.<sup>71</sup> In the second step, assuming the emission mechanism in Fig. 4(c) and using the obtained local fields on the tip apex, emission currents on the tip apex were calculated. In the third step, electron trajectories were simulated where the initial conditions of electron emission on the tip apex were determined by Monte Carlo sampling from the calculated emission current distribution on the tip apex. All simulations were run in a full three-dimensional system that covered the geometry of the counter electrode in front of the tip. During electron propagation, Osterwalder's group included the DC field, the time-dependent laser field as well as the Coulomb fields of all the other emitted electrons and all image charges inside the tip. Finally, in the fourth step, the energy spectrum was recovered from the final velocity distribution of electrons.

The resulting spectra reflect the essential details of the experimental observations. The plateau and the peak features, and their evolution with laser intensity, are well reproduced as shown in Fig. 5(b). The simulations provide a direct insight into the involved electron dynamics. It turned out that, in the strong-field regime, the low-energy peak can only be produced by delayed electron emission. All electrons emitted promptly within the duration of the light pulse contribute to the plateau or its high-energy tail due to the strong space charge effect from mutual Coulomb interactions. A simple delayed-emission model driven by rescattering processes is schematically drawn in Fig. 5(d). The narrowing of the surface barrier induced by the strong laser field induces massive optical field emission from the Fermi level. Driven by the oscillating laser field, a large number of electrons return to the surface with high energy and are re-emitted after typically 50 percent energy loss due to inelastic electron scattering inside the metal. These processes occur within a distance of an inelastic mean free path on the average, which can be of the order of several tens of nanometers in this energy range. The resulting delay times caused by electrons traveling in the metal can thus be tens of femtoseconds, enough to avoid the strong space-charge effects in the promptly emitted electron cloud.



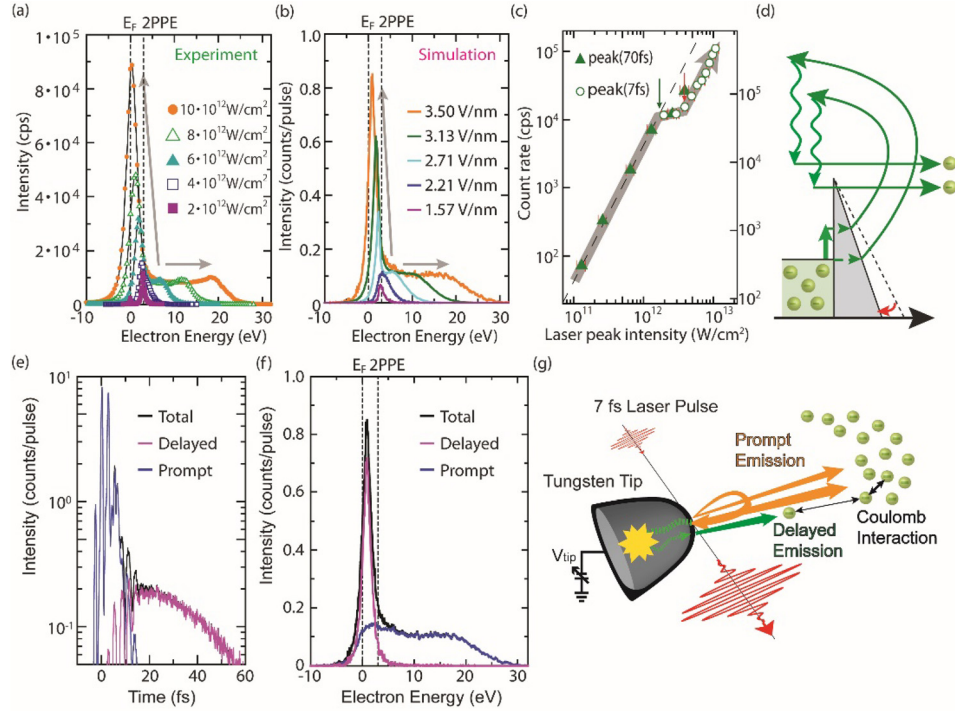


FIG. 5. (a) Experimental and (b) simulated energy spectra for different laser peak intensities. The corresponding laser fields in the simulations represent the maximum laser fields at the focus without field enhancement. The enhancement factor is 2.4 in our case. (c) Evolution of the low-energy peak intensity in the experimental energy spectra, plotted as a function of laser peak intensity including the field enhancement at the tip apex. Filled triangles show peak intensities from an earlier study in the weak-field regime; their count rates are indicated in the vertical axis at the right side. The scale is adjusted such that the level of data points of two different experiments becomes the same around  $2 \times 10^{12} \text{ W/cm}^2$ . The error bars in peak intensities are due to uncertainty in the beam waist at the focus. (d) A schematic diagram of a delayed emission process in the rescattering model. Wavy arrows indicate scattering processes inside the solid that lead to delayed re-emission. (e) Temporal profiles of the electron emission and (f) simulated energy spectra at the counter electrode (pinhole plate); in both panels, the spectra are decomposed into prompt and delayed emission processes. The laser field is 3.5 V/nm. (g) Schematic representation of different emission processes under strong fields, indicated by orange and green arrows. Adapted with permission from Yanagisawa *et al.*, Sci. Rep. 6, 35877 (2016). Copyright 2016 Springer Nature Publishing.

Figure 5(e) shows the temporal profile of the two electron emission channels, an intense prompt emission within the first 10 fs, closely following the oscillations of the laser field, and a much weaker delayed emission during the next tens of femtoseconds. Both emission currents occur within a  $30 \times 30 \text{ nm}^2$  area. Therefore, the prompt emission is spatially and temporally dense enough to produce the broadened energy distribution of the plateau due to the strong Coulomb interaction. Figure 5(f) shows the simulated energy spectrum for the maximum laser field at the tip apex, which decomposed into contributions from the two emission channels. Clearly, the plateau represents the prompt emission and the peak the delayed emission.

The emission processes from a nanoscale metal tip in the strong field regime are summarized in Fig. 5(g). Few-cycle laser pulses with strong enough fields induce massive multiple-electron emission via tunneling from the Fermi level. A fraction of these electrons is driven back to the tip due to the oscillating laser field. Upon colliding with the tip, some of the electrons are elastically rescattered at the very surface. The direct emission and elastically rescattered electrons [orange arrows in Fig. 5(g)] appear within the first ten femtoseconds, and are therefore categorized as prompt emission. They form a dense electron cloud where the strong Coulomb repulsion leads to a massive redistribution of energy and momentum which is reflected in the formation of a featureless plateau in the energy spectrum. In contrast, after re-colliding with the tip, some electrons travel far inside the metal, return to the surface after inelastic scattering, and are re-emitted [green arrows in Fig. 5(g)]. This sequence of processes leads to significant delays with respect to the prompt emission. It is via these delays that the

optical field emission can be disentangled from the concomitant photo-excited electron emission, both temporally and spectrally.

## V. ATTOSECOND DYNAMICS OF THE FRANZ-KELDYSH EFFECT IN DIAMOND

The electric field of an intense optical pulse can drive electron motion in solids at close-to-petahertz frequencies. The resulting dynamics, therefore, unfolds on sub-femtosecond (or attosecond) timescales. These dynamics have become accessible only to direct experimental investigation with the development of attosecond measurement techniques.<sup>72,73</sup> Over the last few years, several aspects of attosecond electron dynamics in bulk solids have been reported in high-profile publications.

Very brief transients of light, covering only one or two oscillations of the underlying carrier wave, have been used to transiently induce conductivity in dielectrics and semiconductors.<sup>34,74</sup> In the original work performed on SiO<sub>2</sub>, very high peak electric fields on the order of 1 V/Å were used to induce electrical currents in this insulator.<sup>34</sup> These very strong fields transiently mix the valence and conduction bands, resulting in a fully reversible increase of the conductivity by many orders of magnitude within less than a femtosecond. In this experiment, the time resolution was obtained by tuning the carrier-envelope offset phase (CEP) of the short light transient. Changing the CEP by  $\pi$  turns, for example, a pulse with the electric field vector at its peak pointing towards the left into a pulse with its peak electric field pointing towards the right. A phase change of  $2\pi$  corresponds to a shift of the carrier wave by one optical oscillation period in time domain—at a center wavelength of 800 nm, this would be  $\approx 2.7$  fs. By monitoring current flow in the dielectric between a “left” and a “right” electrode as a function of fine steps in CEP, Schiffrin and co-workers could therefore resolve how the optical field is able to steer the charges in their sample. In a similar experiment, these methods were recently applied to a GaN sample, where the charge injection mechanism was interpreted as an interference effect of different multi-photon excitation pathways.<sup>74</sup>

Another hot topic in attosecond phenomena driven by strong laser fields in solids is the generation of high-order harmonics of the driving laser frequency. High-harmonics have been generated in solids with mid-infrared driving fields as well as multi-terahertz waves.<sup>75,76</sup> The appearance of the high-harmonic spectra strikingly resembles those familiar from high-harmonic generation in atomic or molecular gases.<sup>77,78</sup> However, it should not be forgotten that the electrons in a solid are moving in a relatively complicated periodic potential rather than just a simple atomic potential. Nevertheless, solid and gas phase harmonics can be linked by considering the generation process in solids, a result of generalized recollisions between the electrons and holes.<sup>79–81</sup>

A third class of attosecond experiments on bulk solids use optical spectroscopic techniques to study strong-field effects. Namely, in attosecond transient absorption spectroscopy (ATAS), where a short, intense near-infrared (NIR) pulse acts as a strong-field pump, and the resulting changes in extreme ultraviolet (XUV) absorbance are probed by a single attosecond pulse or an attosecond pulse train.<sup>82–84</sup> The first experiments have shown that the high-frequency electric fields of the optical pump pulse can drive nonlinear electron dynamics on sub-femtosecond time scales in dielectrics and semiconductors.<sup>35,85–87</sup> This is relevant to practical applications because it tests the ultimate material limit for the high-speed performance of electronic devices that are scaled to smaller and smaller structure sizes and ever higher clock speeds.<sup>88,89</sup>

In particular, Keller’s group used ATAS to investigate a regime of light-matter interaction in a dielectric material where the quiver energy (or ponderomotive energy  $U_p$ ) of the electrons in the oscillating electrical field becomes comparable to the photon energy of the driving laser.<sup>35</sup> In this case, the interaction occurs in an intermediate regime between photon driven (quantum-mechanical) and field driven (classical) interactions. This transition regime between the two well-known limiting cases of quantum and classical mechanics is only little understood. However, while a plethora of phenomena occurs in this parameter range, the importance of intra- versus inter-band transitions for determining the dynamical response of the dielectric has been unclear.

The dynamical Franz-Keldysh effect (DFKE) is an important example of intraband dynamics in this regime<sup>90</sup> [see Figs. 6(a) and 6(b)]. It manifests itself in induced absorption within the bandgap, induced transparency above the band gap and the appearance of optical sidebands. Intuitively, the appearance of these features can be understood by the transient bending of the bands through the external electric field. With the bent bands, the electronic wavefunctions are not unbounded Bloch waves anymore, but now have an exponential (or rather Airy) tail reaching into the forbidden region [Fig. 6(b)]. The DFKE is a nonresonant process in which no real carriers are created—it is therefore expected to be fast. Previously, the DFKE has already been successfully observed in the THz regime (i.e., on picosecond time scales) in the vicinity of the bandgap of semiconductors.<sup>91,92</sup>

In our experiment, Keller's group exposed a 50 nm thick film of polycrystalline diamond to an intense few-femtosecond NIR laser pulse with an intensity of a few times of  $10^{12}$  W/cm<sup>2</sup>. The induced change in absorbance was probed with  $\approx 250$ -as pulses centered at a photon energy of about 42 eV. That means that field-induced effects high up into the conduction band were probed rather than in the proximity of the bandgap. An example of the experimental data is shown in Fig. 6(c). The measured response shows fast oscillations at twice the NIR driving frequency. The phase relation of these oscillations exhibits a non-trivial V-shaped energy dispersion around the main feature centered at 43 eV.

Theoretical analysis of our experiment was performed in collaboration with the group of Yabana from the University of Tsukuba.<sup>35,93,94</sup> *Ab initio* calculations based time-dependent

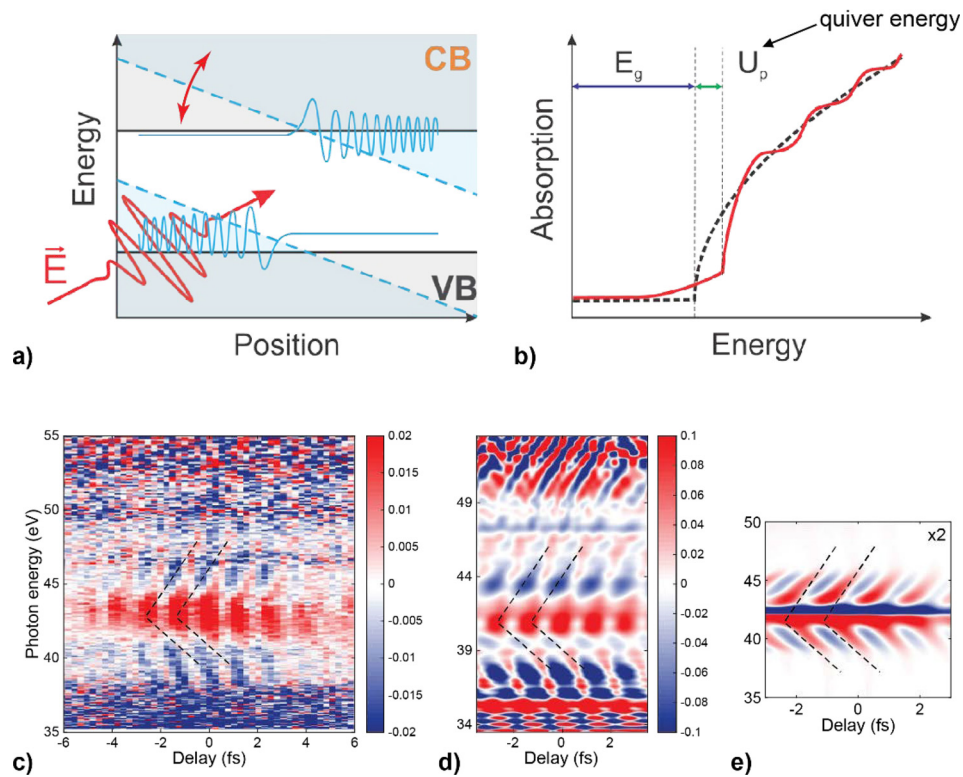


FIG. 6. Dynamical Franz-Keldysh effect (DFKE) in diamond. (a) The oscillating electric field of an intense optical pulse periodically bends the bands of the solid. The electronic states are no longer Bloch states, but have an Airy-tail reaching into the forbidden region. (b) Schematic comparison of the absorbance with DFKE (red line) and the field-free absorbance (dashed black line). The Airy-tail of the wavefunction leads to non-zero absorption below the bandgap. The quiver energy of the electrons in the driving field can be seen as an energetic up-shift of the sharp increase in absorbance above the bandgap. (c) Experimentally measured attosecond transient absorption data. Fast oscillations at twice the carrier frequency of the pump and a V-shaped dispersion of the oscillation phase are clearly visible. (d) Delay-dependent absorbance modeled with time-dependent density functional theory coupled to Maxwell's equation. (e) A simple analytic two-band model assuming parabolic bands still reproduces the main feature and V-shaped dispersion qualitatively. Adapted with permission from Lucchini *et al.*, Science **353**, 916–919 (2016). Copyright 2016 AAAS.

density functional theory (TDDFT) coupled to the Maxwell's equations reproduce the experimental results [Fig. 6(d)]. To identify the origin of the observed response, an orbital decomposition was performed. It was found that one valence band to conduction band transition probed by the XUV attosecond pulse dominates the qualitative behavior of the macroscopic response of diamond in the energy range under examination. Even a simple analytical two-band model, assuming strictly parabolic bands, still reproduces the main feature and V-shaped energy dispersion observed in the experiment [Fig. 6(e)]. This reduction to only two participating bands that are coupled only by the XUV probe pulse allowed us to rule out the contribution of NIR driven interband transitions. It can thus be concluded that intraband processes (the DFKE) dominate the optical response of diamond in our regime of strong-field light-matter interaction.

Our results constitute the first observation of the dynamical Franz-Keldysh effect driven by a few-femtosecond optical pulse and in the middle of the conduction band. While in the 1980s, the rapid development of terahertz wave technologies closed the gap between optics and electronics, we now enter a new regime of field-controlled electronics in the petahertz domain. With the increasing speed of electronic components, it is essential to understand potential physical limitations. The recent results on strong-field driven electron dynamics in solids show that no such limit is to be expected anytime soon with respect to our ability to steer the electrons in materials with electrical fields approaching petahertz frequencies. Furthermore, these experiments pave the way for a new kind of optically assisted spectroscopy of solids with potential to deliver dynamic information on their electronic structure.

## VI. STRONG THz FIELDS AT THE DIRAC POINT OF GRAPHENE

The unique electronic and optical properties of graphene stem from its relativistic low energy band dispersion.<sup>95</sup> Numerous optical studies have investigated the linear optical properties in the THz and infrared regimes,<sup>96–98</sup> showing clear doping controlled THz absorption. Recent progress in THz graphene research has shown that even at modest fields on the order of a few kV/cm, a field dependent increase in transmission can be observed in doped graphene due to a nonlinear response of the excited carriers.<sup>99–104</sup> Whereas in un-doped graphene, where the chemical potential sits close to the Dirac point, a decrease in transmission is observed.<sup>101</sup>

In recent works, the nonlinear optical properties of graphene have been modeled using a phenomenological thermodynamic model for a hot electron gas.<sup>104,105</sup> In particular, in Ref. 10, the heating dynamics of a moderately doped single layer graphene at room temperature ( $E_F = 0.07$  eV and  $T = 300$  K) is reported and reproduced remarkably well using the thermodynamic model. In this simple model, the electronic temperature in graphene is raised due to the conversion of the THz energy into thermal energy. The elevation of the electronic temperature leads to a broadening of the Fermi-Dirac distribution of the electrons and an associated lowering of the chemical potential.

The exceptional conductive properties of graphene drive the search for novel applications. However, previous experiments and the results presented here show that intense terahertz fields compromise the conductivity of graphene, unfavorable for ultrafast high field THz graphene transistors.<sup>106–109</sup> For those applications, it is pivotal to understand and avoid the reduction in conductivity. On the contrary, applications like THz detectors<sup>110,111</sup> rely on the extraction of high-energy electrons into an external circuit. In this case, a high electronic temperature is more critical than the associated reduction in conductivity. The nonlinear optical response of the carriers, and therefore the field dependent reduction of the conductivity and the electronic temperature of the charge carriers, is dependent on the absorption of the THz light by those carriers. As the optical absorption varies with the carrier density of the graphene sheet, the nonlinear THz response of graphene is expected to be strongly doping dependent.<sup>104</sup>

In the present study, the doping dependence of the nonlinear THz response was experimentally investigated. High field THz transmission experiments are performed on back-gated single layer CVD graphene, the area of which is about  $5 \times 5$  mm, well above the THz diffraction limit. With the back-gated device, control over the doping was simultaneously gained with the measure of the transport properties. Terahertz time domain transmission spectra are measured at



temperatures varying from 20 K to room temperature. Terahertz pulses are produced in an organic OH1 crystal pumped with 1300 nm infrared pulses coming from a NOPA. The THz field strength is set with the use of two THz polarizers. After transmission through the sample, a second set of polarizers ensures that the THz field strength and polarization at the ZnTe detection crystal is held constant, guaranteeing a linear electro-optical detection. The maximum THz field strength at the sample position was determined to be 115 kV/cm.

In the limit of low THz fields, the optical response is linear and therefore the time domain spectra can be modeled using a simple Drude model from which the Drude weight and scattering time are extracted.<sup>112</sup> Figure 7(a) shows examples of time domain spectra obtained using a relatively low, 25 kV/cm, and high, 115 kV/cm, field strength. The dashed lines are the best fit to the data using the Drude model,  $\sigma(\omega) = \sigma_0 / (1 - i\omega\tau)$ , where  $\sigma_0 = D\tau/\pi$ ,  $\omega$  is the frequency,  $D$  is the Drude weight and  $\tau$  is the carrier scattering time. Figure 7(b) shows a close-up of the main peak. One can see that at a field strength of 25 kV/cm, the Drude model can reproduce the experimental data strikingly well even though small nonlinearities are expected to affect the transmission. In the limit of low fields and low temperatures, the optical Drude weight  $D$  is directly related to the Fermi energy by  $\hbar D/\sigma_0 = 2|E_F|$ , where  $E_F$  can be found from the transport measurements carried out simultaneously with the optical transmission experiment. In Fig. 7(c), the Drude weight calculated using  $E_F$  obtained from transport measurements is shown (dashed line), while the symbols correspond to  $D$  found by fitting the low field time domain spectra. A remarkable good match between transport and optical measurements is observed. The scattering energy shown in Fig. 7(d) shows no clear dependence on the carrier concentration and is roughly 10 meV, which corresponds to a scattering time  $\tau$  of approximately 400 fs.

The THz response of the gated graphene sample was determined using THz fields of up to 115 kV/cm and different doping levels established by the back-gate. The response of graphene was analyzed by extracting the peak-to-peak electric field of the main peak in time domain

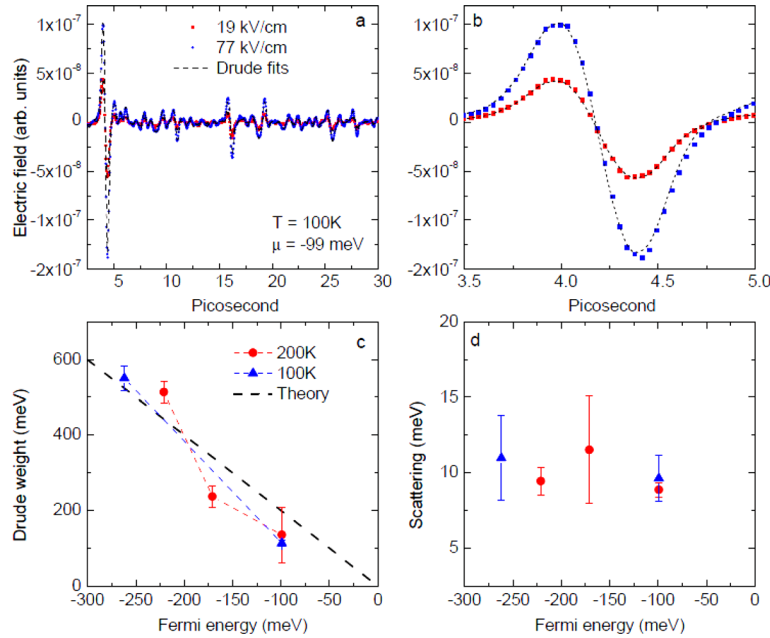


FIG. 7. Low THz field transmission analyzed using the Drude model. (a) Low and high field THz time domain spectra transmitted by the graphene sample, showing the main peak and two echo's originating from Fabry-Perot oscillations in the silicon substrate. (b) A close-up of the main peak of the spectra shown in panel (a). The symbols correspond to the experimental curves; the black dashed lines are fits using the Drude model. (c) The Drude weight as a function of Fermi energy and at different temperatures, found from Drude fitting, is shown as symbols, the dashed line is the theoretical weight based on the extracted Fermi energy. (d) The doping dependence of the scattering energy obtained from the Drude fitting. The error bars in (c) and (d) are estimated by taking the standard deviation of several fit results using various initial conditions of  $D$  and  $\tau$ .



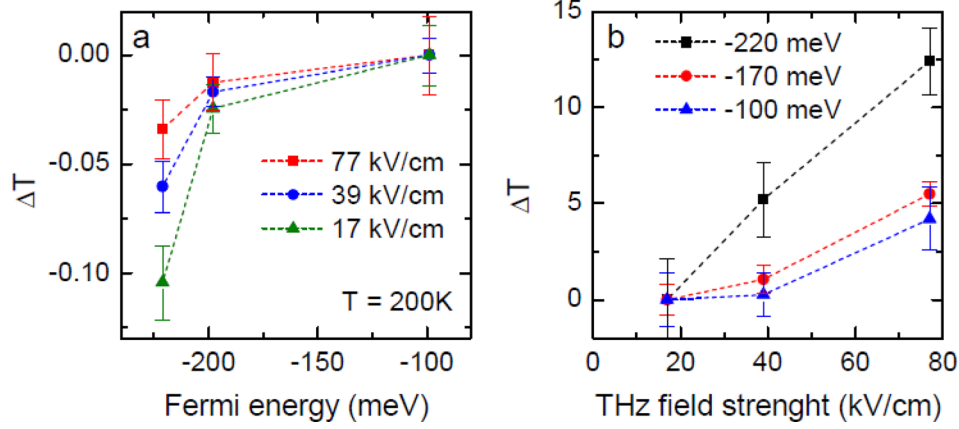


FIG. 8. Normalized transmission as a function of Fermi energy and THz field. (a) The transmission normalized to the smallest carrier concentration at  $T = 200$  K, as a function of Fermi energy for three different THz field strengths. (b) The transmission normalized to the smallest THz field strength at  $T = 200$  K, as a function of THz field.

spectra. The peak-to-peak electric field transmitted by the graphene on the substrate was then normalized to the peak-to-peak electric field of the pristine pulse for each THz field. This results in a value,  $\Delta T(E_F, FS) = \Delta T_{\text{graphene}}(E_F, FS) / \Delta T_{\text{THz pulse}}(FS)$ , for each Fermi energy  $E_F$  and THz field strength  $FS$ .

Figure 8(a) shows the transmission for three different THz field strengths, each normalized to the transmission at the lowest carrier concentration:  $\Delta T_{EF}(E_F, FS) = [\Delta T(E_F, FS) - \Delta T(E_{F,\min}, FS)] / \Delta T(E_{F,\min}, FS)$ . At higher Fermi energy, more free carriers are present in the graphene layer, therefore the Drude absorption should increase and thus the transmission decreases. Indeed,  $\Delta T(E_F)$  is clearly reduced at high Fermi energies for all THz field strengths. The observed decrease is as much as  $\sim 11\%$ , for weak THz field strength. For higher THz field strengths, the maximal change in  $\Delta T(E_F)$  is reduced to less than  $-3\%$ . The high THz fields are counteracting the effect of the gate on the optical properties of the graphene layer, although it was not possible to go to high enough doping levels where the effect of the THz field overtakes the influence of the gate.

Figure 8(b) shows the transmission for three different doping levels, each normalized to the transmission at the corresponding lowest THz field strength:  $\Delta T_{FS}(E_F, FS) = [\Delta T(E_F, FS) - \Delta T(E_F, FS_{\min})] / \Delta T(E_F, FS_{\min})$ . For low Fermi energy, a small increase in transmission, of about 4%, is observed when increasing the THz field which is the saturable absorption observed in previous studies. Importantly, upon increasing the Fermi energy, the maximal observed increase in transmission becomes significantly larger (6% and 12.5%), showing that the relative reduction of conductivity, and therefore the nonlinear response, increases together with the carrier concentration.

Our experimental results show that the THz induced nonlinearities are more pronounced for high sample doping. At the same time, the THz field mitigates the effect of the gate on the conductivity. The increased transmission is observed for all doping levels, even close to the Dirac point, which is in agreement with that reported in previous studies for highly doped graphene.<sup>100,104,113–115</sup> But, we do not corroborate the positive change in photoconductivity observed in an optical pump-THz probe study on low doped graphene.<sup>114</sup>

The experimental results show that the THz field induced saturable absorption is more pronounced for high sample doping. This is in direct disagreement with the expected doping dependence based on the phenomenological thermodynamic model.<sup>104</sup>

## VII. CONCLUSION

Optical fields with amplitudes comparable to or exceeding the atomic binding fields lead to a wealth of novel and fascinating phenomena like the generation of attosecond optical and

electronic bursts, new “photo-atoms” with associated quantized states, the ability of transforming insulators into conductors, or materials into high T<sub>c</sub> superconductors, etc. With the current development of ultrahigh power (PW to EW class) laser facilities, intense THz sources, and XFELs, the strong field manipulation of matter is today in its starting phase only, but is promising to have an “ultra-bright” future.

## ACKNOWLEDGMENTS

The authors acknowledge support from the NCCR “MUST” (Molecular Ultrafast Science and Technology) of the Swiss National Science Foundation.

- <sup>1</sup>G. Floquet, *Ann. Éc. Norm. Supér.* **12**, 47–88 (1883).
- <sup>2</sup>S. H. Autler and C. H. Townes, *Phys. Rev.* **100**(2), 703 (1955).
- <sup>3</sup>R. J. Levis, G. M. Menkir, and H. Rabitz, *Science* **292**, 709 (2001).
- <sup>4</sup>P. M. Kraus, O. I. Tolstikhin, D. Baykusheva, A. Rupenyan, J. Schneider, C. Z. Bisgaard, T. Morishita, F. Jensen, L. B. Madsen, and H. J. Wörner, *Nat. Commun.* **6**, 7039 (2015).
- <sup>5</sup>Review from U. Keller.
- <sup>6</sup>P. Corkum, *Phys. Rev. Lett.* **71**(13), 1994 (1993).
- <sup>7</sup>Q. Su, J. H. Eberly, and J. Javanainen, *Phys. Rev. Lett.* **64**(8), 862 (1990).
- <sup>8</sup>M. Pont and M. Gavrila, *Phys. Rev. Lett.* **65**(19), 2362 (1990).
- <sup>9</sup>A. Scrinzi, N. Elander, and B. Piraux, *Phys. Rev. A* **48**, R2527 (1993).
- <sup>10</sup>M. Y. Ivanov, O. V. Tikhonova, and M. V. Fedorov, *Phys. Rev. A* **58**(2), R793 (1998).
- <sup>11</sup>E. A. Volkova, A. M. Popov, O. V. Smirnova, and O. V. Tikhonova, *J. Exp. Theor. Phys.* **84**, 658–664 (1997).
- <sup>12</sup>T. Nubbemeyer, K. Gorling, A. Saenz, U. Eichmann, and W. Sandner, *Phys. Rev. Lett.* **101**(23), 233001 (2008).
- <sup>13</sup>U. Eichmann, A. Saenz, S. Eilzer, T. Nubbemeyer, and W. Sandner, *Phys. Rev. Lett.* **110**(20), 203002 (2013).
- <sup>14</sup>M. Matthews, T. Bredtmann, A. Patas, A. Lindinger, J. Gateau, S. Hermelin, J. Kasparian, M. Richter, O. Smirnova, F. Morales, J.-P. Wolf, and M. Ivanov, “Amplification of intense light fields by ‘bound states of free electrons,’” *Nat. Phys.* (submitted).
- <sup>15</sup>T. Higuchi, L. Maisenbacher, A. Liehl, P. Dombi, and P. Hommelhoff, *App. Phys. Lett.* **106**, 051109 (2015).
- <sup>16</sup>M. Kruger, M. Schenk, and P. Hommelhoff, *Nature (London)* **475**, 78 (2011).
- <sup>17</sup>G. Herink, D. R. Solli, M. Gulde, and C. Ropers, *Nature (London)* **483**, 190 (2012).
- <sup>18</sup>H. Yanagisawa, S. Schnepp, C. Hafner, M. Hengsberger, D. E. Kim, M. F. Kling, A. Landsman, L. Gallmann, and J. Osterwalder, *Sci. Rep.* **6**, 35877 (2016).
- <sup>19</sup>A. Zavriyev, P. Bucksbaum, J. Squier, and F. Salane, *Phys. Rev. Lett.* **70**, 1077 (1993).
- <sup>20</sup>P. H. Bucksbaum, A. Zavriyev, H. G. Muller, and D. W. Schumacher, *Phys. Rev. Lett.* **64**, 1883 (1990).
- <sup>21</sup>J.-M. Yuan and T. F. George, *J. Chem. Phys.* **68**, 3040 (1978).
- <sup>22</sup>A. D. Bandrauk, *Molecules in Laser Fields* (Marcel Dekker, New York, 1994).
- <sup>23</sup>B. M. Garraway and K.-A. Suominen, *Phys. Rev. Lett.* **80**, 932 (1998).
- <sup>24</sup>M. Rodriguez, K.-A. Suominen, and B. Garraway, *Phys. Rev. A* **62**, 053413 (2000).
- <sup>25</sup>M. Sindelka, N. Moiseyev, and L. S. Cederbaum, *J. Phys. B* **44**(4), 045603 (2011).
- <sup>26</sup>P. V. Demekhin and L. S. Cederbaum, *J. Chem. Phys.* **139**(15), 154314 (2013).
- <sup>27</sup>M. E. Corrales, J. Gonzalez-Vazquez, G. Balerdi, I. R. Sola, R. de Nalda, and L. Banares, *Nat. Chem.* **6**, 785 (2014).
- <sup>28</sup>I. R. Sola, J. Gonzalez-Vazquez, R. de Nalda, and L. Banares, *Phys. Chem. Chem. Phys.* **17**, 13183 (2015).
- <sup>29</sup>A. Natan, M. R. Ware, V. S. Prabhudesai, U. Lev, B. D. Bruner, O. Heber, and P. H. Bucksbaum, *Phys. Rev. Lett.* **116**, 143004 (2016).
- <sup>30</sup>B. J. Sussman, D. Townsend, M. Y. Ivanov, and A. Stolow, *Science* **314**, 278 (2006).
- <sup>31</sup>J. Kim, H. Tao, J. L. White, V. S. Petrović, T. J. Martinez, and P. H. Bucksbaum, *J. Phys. Chem. A* **116**, 2758 (2012).
- <sup>32</sup>Y. Mizumoto, Y. Kayanuma, A. Srivastava, J. Kono, and A. H. Chin, *Phys. Rev. B* **74**(4), 045216 (2006).
- <sup>33</sup>M. Holthaus, *Phys. Rev. Lett.* **69**, 351 (1992).
- <sup>34</sup>A. Schiffrin, T. Paasch-Colberg, N. Karpowicz, V. Apalkov, D. Gerster, S. Muhlbrandt, M. Korbman, J. Reichert, M. Schultze, S. Holzner, J. V. Barth, R. Kienberger, R. Ernstorfer, V. S. Yakovlev, M. I. Stockman, and F. Krausz, *Nature* **493**(7430), 70–74 (2013).
- <sup>35</sup>M. Lucchini, S. A. Sato, A. Ludwig, J. Herrmann, M. Volkov, L. Kasmi, Y. Shinohara, K. Yabana, L. Gallmann, and U. Keller, *Science* **353**(6302), 916 (2016).
- <sup>36</sup>H. Niikura, F. Légaré, R. Hasbani, A. D. Bandrauk, M. Yu. Ivanov, D. M. Villeneuve, and P. B. Corkum, *Nature* **417**, 917 (2002).
- <sup>37</sup>H. Niikura, F. Légaré, R. Hasbani, M. Ivanov, D. M. Villeneuve, and P. B. Corkum, *Nature* **421**, 826 (2003).
- <sup>38</sup>M. Lein, *Phys. Rev. Lett.* **94**, 053004 (2005).
- <sup>39</sup>S. Baker, J. S. Robinson, C. A. Haworth, H. Teng, R. A. Smith, C. C. Chirila, M. Lein, J. W. G. Tisch, and J. P. Marangos, *Science* **312**, 424 (2006).
- <sup>40</sup>P. M. Kraus and H. J. Wörner, *ChemPhysChem* **14**(7), 1445–1450 (2013).
- <sup>41</sup>C. I. Baga, J. Xu, A. D. DiChiara, E. Sistrunk, K. Zhang, P. Agostini, T. A. Miller, L. F. DiMauro, and C. D. Lin, *Nature* **483**, 194 (2012).
- <sup>42</sup>O. Smirnova, Y. Mairesse, S. Patchkovskii, N. Dudovich, D. M. Villeneuve, P. B. Corkum, and M. Y. Ivanov, *Nature* **460**(7258), 972–977 (2009).
- <sup>43</sup>S. Haessler, J. Caillat, W. Boutu, C. Giovanetti-Teixeira, T. Ruchon, T. Auguste, Z. Diveki, P. Breger, A. Maquet, B. Carré, R. Taieb, and P. Salières, *Nat. Phys.* **6**(3), 200–206 (2010).

- <sup>44</sup>P. M. Kraus, B. Mignolet, D. Baykusheva, A. Rupenyan, L. Horný, E. F. Penka, G. Grassi, O. I. Tolstikhin, J. Schneider, F. Jensen, L. B. Madsen, A. D. Bandrauk, F. Remacle, and H. J. Wörner, *Science* **350**, 790–795 (2015).
- <sup>45</sup>P. M. Kraus, Y. Arasaki, J. B. Bertrand, S. Patchkovskii, P. B. Corkum, D. M. Villeneuve, K. Takatsuka, and H. J. Wörner, *Phys. Rev. A* **85**, 043409 (2012).
- <sup>46</sup>P. M. Kraus, D. Baykusheva, and H. J. Wörner, *Phys. Rev. Lett.* **113**, 023001 (2014).
- <sup>47</sup>P. M. Kraus, D. Baykusheva, and H. J. Wörner, *J. Phys. B* **47**, 124030 (2014).
- <sup>48</sup>L. Bergé, S. Skupin, R. Nuter, J. Kasparian, and J. P. Wolf, *Rep. Prog. Phys.* **70**, 1633–1713 (2007).
- <sup>49</sup>P. Béjot, E. Cormier, E. Hertz, B. Lavorel, J. Kasparian, J.-P. Wolf, and O. Faucher, *Phys. Rev. Lett.* **110**, 043902 (2013).
- <sup>50</sup>P. Béjot, J. Kasparian, S. Henin, V. Loriot, T. Vieillard, E. Hertz, O. Faucher, B. Lavorel, and J.-P. Wolf, *Phys. Rev. Lett.* **104**, 103903 (2010).
- <sup>51</sup>J. H. Eberly and K. C. Kulander, *Science* **262**(5137), 1229–1233 (1993).
- <sup>52</sup>M. Richter, S. Patchkovskii, F. Morales, O. Smirnova, and M. Ivanov, *New J. Phys.* **15**(8), 083012 (2013).
- <sup>53</sup>F. Morales, M. Richter, S. Patchkovskii, and O. Smirnova, *Proc. Natl. Acad. Sci. U.S.A.* **108**, 16906 (2011).
- <sup>54</sup>M. Gavrila, I. Simbotin, and M. Stroe, *Phys. Rev. A* **78**, 033404 (2008).
- <sup>55</sup>E. Mede and R. M. Potvliege, *Laser Phys. Lett.* **4**(5), 357 (2007).
- <sup>56</sup>W. C. Henneberger, *Phys. Rev. Lett.* **21**, 838 (1968).
- <sup>57</sup>M. Gavrila, *J. Phys. B: At. Mol. Opt. Phys.* **35**, R147 (2002).
- <sup>58</sup>U. Eichmann, T. Nubbemeyer, H. Rottke, and W. Sandner, *Nature* **461**, 1261–1264 (2009).
- <sup>59</sup>A. M. Popov, O. V. Tikhonova, and E. A. Volkova, *J. Mod. Opt.* **58**, 1195 (2011).
- <sup>60</sup>V. Kapoor and D. Bauer, *Phys. Rev. A* **85**, 023407 (2012).
- <sup>61</sup>W. Ettoumi, Y. Petit, J. Kasparian, and J.-P. Wolf, *Opt. Express* **18**(7), 6613–6620 (2010).
- <sup>62</sup>C. Ott, A. Kaldun, P. Raith, K. Meyer, M. Laux, J. Evers, C. H. Keitel, C. H. Greene, and T. Pfeifer, *Science* **340**(6133), 716–720 (2013).
- <sup>63</sup>R. Gomer, *Field Emission and Field Ionization* (AIP, New York, 1993).
- <sup>64</sup>K. Nagaoka *et al.*, *Nature (London)* **396**, 557 (1998).
- <sup>65</sup>B. Cho *et al.*, *Phys. Rev. Lett.* **92**, 246103 (2004).
- <sup>66</sup>P. Hommelhoff, Y. Sortais, A. Aghajani-Talesh, and M. A. Kasevich, *Phys. Rev. Lett.* **96**, 077401 (2006).
- <sup>67</sup>D. Ehberger *et al.*, *Phys. Rev. Lett.* **114**, 227601 (2015).
- <sup>68</sup>H. Yanagisawa, C. Hafner, P. Dona, M. Klöckner, D. Leuenberger, T. Greber, M. Hengsberger, and J. Osterwalder, *Phys. Rev. Lett.* **103**, 257603 (2009).
- <sup>69</sup>L. Wu and L. K. Ang, *Phys. Rev. B* **78**, 224112 (2008).
- <sup>70</sup>H. Yanagisawa, M. Hengsberger, D. Leuenberger, M. Klöckner, C. Hafner, T. Greber, and J. Osterwalder, *Phys. Rev. Lett.* **107**, 087601 (2011).
- <sup>71</sup>C. Hafner, see <http://openmax.ethz.ch/> for OpenMaXwell, 2014.
- <sup>72</sup>F. Krausz and M. Ivanov, *Rev. Mod. Phys.* **81**, 163 (2009).
- <sup>73</sup>L. Gallmann, C. Cirelli, and U. Keller, *Annu. Rev. Phys. Chem.* **63**, 447–469 (2012).
- <sup>74</sup>T. Paasch-Colberg, S. Y. Kruchinin, Ö. Saglam, S. Kapser, S. Cabrini, S. Muehlbrandt, J. Reichert, J. V. Barth, R. Ernstorfer, R. Kienberger, V. S. Yakovlev, N. Karpowicz, and A. Schiffrin, *Optica* **3**, 1358–1361 (2016).
- <sup>75</sup>S. Ghimire, A. D. DiChiara, E. Sistrunk, P. Agostini, L. F. DiMauro, and D. A. Reis, *Nat. Phys.* **7**, 138–141 (2011).
- <sup>76</sup>O. Schubert, M. Hohenleutner, F. Langer, B. Urbaneck, C. Lange, U. Huttner, D. Golde, T. Meier, M. Kira, S. W. Koch, and R. Huber, *Nat. Photonics* **8**, 119–123 (2014).
- <sup>77</sup>M. Ferray, A. L’Huillier, X. F. Li, L. A. Lompré, G. Mainfray, and C. Manus, *J. Phys. B: At. Mol. Opt. Phys.* **21**, L31–L35 (1988).
- <sup>78</sup>A. McPherson, G. Gibson, H. Jara, U. Johann, T. S. Luk, I. A. McIntyre, K. Boyer, and C. K. Rhodes, *J. Opt. Soc. Am. B* **4**, 595–601 (1987).
- <sup>79</sup>G. Vampa, T. J. Hammond, N. Thiré, B. E. Schmidt, F. Légaré, C. R. McDonald, T. Brabec, and P. B. Corkum, *Nature* **522**, 462–464 (2015).
- <sup>80</sup>M. Garg, M. Zhan, T. T. Luu, H. Lakhotia, T. Klostermann, A. Guggenmos, and E. Goulielmakis, *Nature* **538**, 359–363 (2016).
- <sup>81</sup>T. T. Luu and H. J. Wörner, *Phys. Rev. B* **94**, 115164 (2016).
- <sup>82</sup>E. Goulielmakis, Z.-H. Loh, A. Wirth, R. Santra, N. Rohringer, V. S. Yakovlev, S. Zherebtsov, T. Pfeifer, A. M. Azezer, M. F. Kling, S. R. Leone, and F. Krausz, *Nature* **466**, 739–743 (2010).
- <sup>83</sup>H. Wang, M. Chini, S. Chen, C.-H. Zhang, F. He, Y. Cheng, Y. Wu, U. Thumm, and Z. Chang, *Phys. Rev. Lett.* **105**, 143002 (2010).
- <sup>84</sup>M. Holler, F. Schapper, L. Gallmann, and U. Keller, *Phys. Rev. Lett.* **106**, 123601 (2011).
- <sup>85</sup>M. Schultze, E. M. Bothschafter, A. Sommer, S. Holzner, W. Schweinberger, M. Fiess, M. Hofstetter, R. Kienberger, V. Apalkov, V. S. Yakovlev, M. I. Stockman, and F. Krausz, *Nature* **493**, 75–78 (2013).
- <sup>86</sup>M. Schultze, K. Ramasesha, C. D. Pemmaraju, S. A. Sato, D. Whitmore, A. Gandman, J. S. Prell, L. J. Borja, D. Prendergast, K. Yabana, D. M. Neumark, and S. R. Leone, *Science* **346**, 1348–1352 (2014).
- <sup>87</sup>H. Mashiko, K. Oguri, T. Yamaguchi, A. Suda, and H. Gotoh, *Nat. Phys.* **12**, 741–745 (2016).
- <sup>88</sup>F. Krausz and M. I. Stockman, *Nat. Photonics* **8**, 205–213 (2014).
- <sup>89</sup>H. J. Caulfield and S. Dolev, *Nat. Photonics* **4**, 261–263 (2010).
- <sup>90</sup>A. P. Jauho and K. Johnsen, *Phys. Rev. Lett.* **76**, 4576–4579 (1996).
- <sup>91</sup>K. B. Nordstrom, K. Johnsen, S. J. Allen, A.-P. Jauho, B. Birnir, J. Kono, T. Noda, H. Akiyama, and H. Sakaki, *Phys. Rev. Lett.* **81**, 457–460 (1998).
- <sup>92</sup>F. Novelli, D. Fausti, F. Giusti, F. Parmigiani, and M. Hoffmann, *Sci. Rep.* **3**, 1227 (2013).
- <sup>93</sup>S. A. Sato, K. Yabana, Y. Shinohara, T. Otobe, and G. F. Bertsch, *Phys. Rev. B* **89**, 064304 (2014).
- <sup>94</sup>T. Otobe, Y. Shinohara, S. A. Sato, and K. Yabana, *Phys. Rev. B* **93**, 045124 (2016).
- <sup>95</sup>K. S. Novoselov, A. K. Geim, S. V. Morozov, D. Jiang, S. V. Dubonos, I. V. Grigorieva, and A. A. Firsov, *Science* **306**, 666 (2004).

- <sup>96</sup>K. F. Mak, M. Y. Sfeir, Y. Wu, C. H. Lui, J. A. Misewich, and T. F. Heinz, *Phys. Rev. Lett.* **101**, 196405 (2008).
- <sup>97</sup>J. Horng, C.-F. Chen, B. Geng, C. Girit, Y. Zhang, Z. Hao, H. A. Bechtel, M. Martin, A. Zettl, M. F. Crommie *et al.*, *Phys. Rev. B* **83**, 165113 (2011).
- <sup>98</sup>A. J. Frenzel, C. H. Lui, Y. C. Shin, J. Kong, and N. Gedik, *Phys. Rev. Lett.* **113**, 056602 (2014).
- <sup>99</sup>A. J. Frenzel, *Appl. Phys. Lett.* **102**, 113111 (2013).
- <sup>100</sup>H. Y. Hwang, *J. Phys. Chem. B* **117**, 15819 (2013).
- <sup>101</sup>M. J. Paul *et al.*, *New J. Phys.* **15**, 085019 (2013).
- <sup>102</sup>M. J. Paul, *Appl. Phys. Lett.* **105**, 221107 (2014).
- <sup>103</sup>H. Razavipour, W. Yang, A. Guermoune, M. Hilke, D. G. Cooke, I. Al-Naib, M. M. Dignam, F. m c. Blanchard, H. A. Hafez, X. Chai *et al.*, *Phys. Rev. B* **92**, 245421 (2015).
- <sup>104</sup>Z. Mics, K.-J. Tielrooij, K. Parvez, S. A. Jensen, I. Ivanov, X. Feng, K. Mllen, M. Bonn, and D. Turchinovich, *Nat. Commun.* **6**, 7655 (2015).
- <sup>105</sup>S. A. Jensen, *Nano Lett.* **14**, 5839 (2014).
- <sup>106</sup>F. Schwierz, *Nat. Nanotechnol.* **5**, 487 (2010).
- <sup>107</sup>Y. Wu, *Nature* **472**, 74 (2011).
- <sup>108</sup>R. Cheng, *Proc. Natl Acad. Sci. U.S.A.* **109**, 11588 (2012).
- <sup>109</sup>N. M. Gabor, *Science* **334**, 648 (2011).
- <sup>110</sup>M. Mittendorff, *Appl. Phys. Lett.* **103**, 021113 (2013).
- <sup>111</sup>X. Cai, *Nat. Nanotechnol.* **9**, 814 (2014).
- <sup>112</sup>A. B. Kuzmenko, *Rev. Sci. Instrum.* **76**, 083108 (2005).
- <sup>113</sup>K. J. Tielrooij, J. C. W. Song, S. A. Jensen, A. Centeno, A. Pesquera, A. Zurutuza Elorza, M. Bonn, L. S. Levitov, and F. H. L. Koppens, *Nat. Phys.* **9**, 248 (2013).
- <sup>114</sup>S. Shi, *Nano Lett.* **14**, 1578 (2014).
- <sup>115</sup>J. N. Heyman, J. D. Stein, Z. S. Kaminski, A. R. Banman, A. M. Massari, and J. T. Robinson, *J. Appl. Phys.* **117**, 015101 (2015).
- <sup>116</sup>K. A. Pronin and A. D. Bandrauk, *Phys. Rev. B* **50**, 3473 (1994).
- <sup>117</sup>M. Sivilis, M. Taucer, G. Vampa, K. Johnston, A. Staudte, A. Y. Naumov, D. M. Villeneuve, C. Ropers, and P. B. Corkum, *Science* **357**, 303 (2017).